Journal of Power Sources 255 (2014) 294–301

Contents lists available at ScienceDirect

Journal of Power Sources

journal homepage: www.elsevier.com/locate/jpowsour

Thermal runaway features of large format prismatic lithium ion battery using extended volume accelerating rate calorimetry

Xuning Feng [a], Mou Fang [b], Xiangming He [a,b], Minggao Ouyang [a,*], Languang Lu [a], Hao Wang [b], Mingxuan Zhang [a]

[a] State Key Laboratory of Automotive Safety and Energy, Tsinghua University, Beijing 100084, China
[b] Institute of Nuclear and New Energy Technology, Tsinghua University, Beijing 100084, China

HIGHLIGHTS

- Thermal runaway behavior of a 25 Ah prismatic Li-ion battery is evaluated using ARC.
- When thermal runaway happens, the temperature inside the battery is 870 °C or so.
- When thermal runaway happens, the temperature difference within the battery is 520 °C.
- The internal resistance is got by pulse current charging during thermal runaway test.
- The sharp drop of voltage is 15–40 s sooner than the sudden rise of temperature.

ARTICLE INFO

Article history:
Received 9 October 2013
Received in revised form
27 December 2013
Accepted 1 January 2014
Available online 8 January 2014

Keywords:
Lithium ion battery
Thermal runaway
Large format
Extended volume accelerating rate calorimetry

ABSTRACT

In this paper, the thermal runaway features of a 25 Ah large format prismatic lithium ion battery with $Li(Ni_xCo_yMn_z)O_2$ (NCM) cathode are evaluated using the extended volume-accelerating rate calorimetry (EV-ARC). 4 thermocouples are set at different positions of the battery. The temperature inside the battery is 870 °C or so, much higher than that outside the battery. The temperature difference is calculated from the recorded data. The temperature difference within the battery stays lower than 1 °C for 97% of the test period, while it rises to its highest, approximately 520 °C, when thermal runaway happens. The voltage of the battery is also measured during the test. It takes 15–40 s from the sharp drop of voltage to the instantaneous rise of temperature. Such a time interval is beneficial for early warning of the thermal runaway. Using a pulse charge/discharge profile, the internal resistance is derived from the quotient of the pulse voltage and the current during the ARC test. The internal resistance of the battery increases slowly from 20 mΩ to 60 mΩ before thermal runaway, while it rises to 370 mΩ when thermal runaway happens indicating the loss of the integrity of the separator or the battery swell.

1. Introduction

Currently, lithium ion batteries are favored by researchers as a promising power source for electric vehicles (EVs). However, some hazards of the lithium ion battery have been reported [1]. The safety problems will undermine the confidence of the consumers and obstruct the commercialization of the EVs. Thus the safety issue of the lithium ion battery merits further study.

The thermal runaway behaviors of lithium ion battery have been reviewed several times [2–5]. Generally, when the temperature reaches approximately 90 °C, the self heating of the cell begins due to the start of the solid electrolyte interface (SEI) decomposition. Then follows the negative active material and electrolyte reaction, positive active material and electrolyte reaction, electrolyte decomposition, negative active material and binder reaction, etc. [1–6].

Accelerating rate calorimetry (ARC) is designed to study the exothermic chemical reactions by simulating an adiabatic condition [7]. Employing the ARC, some of the critical kinetic parameters, i.e. the onset temperature of the reaction and the enthalpy of the exothermic process, can be acquired. Not only has ARC been used to analyze the thermal behaviors of the components of the lithium ion battery [8–12], but also to evaluate the thermal hazard of the whole battery [13–15]. Shu and his group have completed a series of thermal abuse tests using a calorimetry named vent size package 2 (VSP2) [16–20], of which the functions are quite the same as those of the ARC.

* Corresponding author. Tel.: +86 10 62773437; fax: +86 10 62785708.
E-mail addresses: fxn07@mails.tsinghua.edu.cn, xuning.feng@qq.com (X. Feng), ouymg@tsinghua.edu.cn (M. Ouyang).

0378-7753/$ – see front matter © 2014 Elsevier B.V. All rights reserved.
http://dx.doi.org/10.1016/j.jpowsour.2014.01.005

One single cell cannot meet the requirements of power and energy for the EVs, so it is a must to build battery packs with hundreds of single cells connected in parallel and series [21–24]. Large format lithium ion batteries are rapidly being developed to provide an alternative for the pack design [25,26]. Lithium ion cells with increased format have the advantage of reducing the number of basic units when integrated in a battery pack [27]. Reducing the number of cells increases reliability because the cells can be connected in series [28]. Thus some of the manufacturers of electric vehicles are favoring large format lithium ion battery.

However, the thermal behaviors of the scaled-up lithium ion batteries mutate under safety incidents, comparing with that of the small-sized cells [29]. A larger format battery is more vulnerable to thermal runaway because it contains more stored energy. The cooling performance is worse due to its lower surface:volume ratio. In addition, the scaled-up size leads to an increase of temperature difference within the battery [28]. Sensors, especially the thermocouples, have been employed to study the internal temperature and the temperature distribution of the lithium ion batteries [30–34]. The temperature difference within the battery is less than approximately 10 °C as reported in Refs. [31–34]. Kim [27,28] et al. have built models to simulate the temperature distribution of a large format cylindrical battery. The simulated temperature difference for normal operation condition is 10 °C or so [27]. However, for thermal runaway triggered by an internal short circuit, the temperature difference is approximately 600 °C [28].

Until now, little research has been done on evaluating the thermal runaway features of large format lithium ion battery. Most of the existing experiments are conducted for 18,650 cells [14–20], or for batteries with a capacity of less than 1 Ah [13]. Models of the large format lithium ion battery are calling for experimental validation [27,28]. The size of the calorimetry restricted the former research on the large format lithium ion battery. Now Thermal Hazard Technology (THT) has developed a new type of ARC named extended volume-ARC (the EV-ARC). The EV-ARC provides a possible solution to test large samples, including the large format lithium ion battery [7].

In the Vehicle Battery Safety Roadmap Guidance [35], Dr. Doughty and Dr. Pesaran synthesized the performance of cells with variant cathode materials, i.e. $LiCoO_2$ (LCO), $LiNi_{0.8}Co_{0.15}Al_{0.05}O_2$ (NCA), $Li(Ni_{1/3}Co_{1/3}Mn_{1/3})_{0.9}O_2$ (NCM), $LiMn_2O_4$ (LMO) and $LiFePO_4$ (LFP). The cell with NCM cathode performs better in thermal runaway tests than those with the LCO and the NCA do, while it performs worse than those with the LMO and LFP do. However, the cell with NCM cathode has better high temperature durability and higher specific capacity than that with the LMO cathode does. Also the cell with NCM cathode costs less and has higher energy density than that with the LFP cathode does. Therefore cells with NCM cathode are of interest to be used in the recent applications of battery pack for electric vehicle.

In this paper, a 25 Ah prismatic battery with NCM cathode is tested by the EV-ARC. The thermal runaway features of the 25 Ah battery have been reported synthetically. The inside temperature has been recorded and the temperature difference within the battery during the thermal runaway process has been reported. The battery voltage is recorded, and the internal resistance is measured by exerting a pulse charging on the sample during the ARC test.

2. Experiment

2.1. The EV-ARC

The instrument used is the es-ARC with double systems, including a standard ARC and an EV-ARC, manufactured by THT, Fig. 1. The functions of the EV-ARC are quite the same as those pervasively used ARC. A common EV-ARC test also follows the heat-wait-seek method. The difference is that the calorimeter of the EV-ARC is much larger than that of the standard ARC. The calorimeter of the standard ARC has an internal size of 10 cm diameter by 10 cm depth, while the calorimeter of the EV-ARC has an internal size of 25 cm diameter and 50 cm depth.

Fig. 1. The illustration of the es-ARC with double systems made by the THT.

2.2. The 25 Ah NCM battery

The 25 Ah battery employed for the EV-ARC test is manufactured by AE Energy Co. Ltd. with NCM/Graphite as its electrodes. Fig. 2 shows the product dimensions of the 25 Ah NCM battery. Remember that the standard ARC calorimeter has an internal size of 10 cm diameter by 10 cm depth. The 25 Ah battery is too large to be held in the standard ARC.

Fig. 3 shows the C/5 (5 A) charging curve of the 25 Ah NCM battery.

2.3. The experiment settings

The 25 Ah battery is composed of two pouch cells connected in parallel wrapped by an aluminum shell, Fig. 4. The structure provides a convenience to insert a micro-thermocouple between the two pouch cells. Though the cover and the shell were separated, the

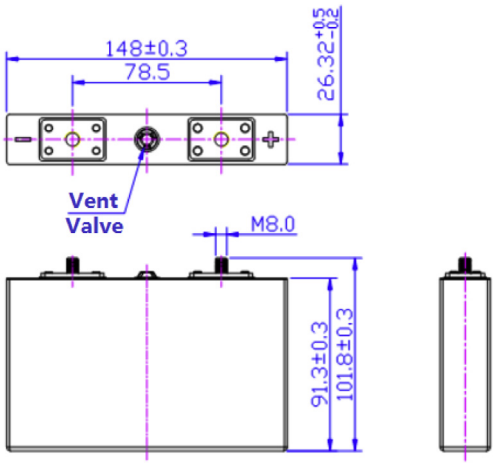

Fig. 2. The product dimensions of the 25 Ah NCM battery.

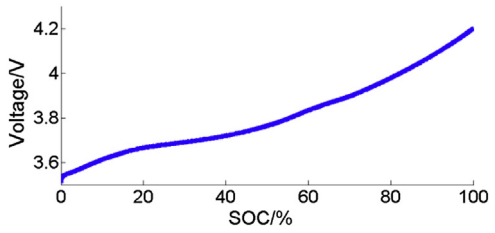

Fig. 3. The C/5 charging curve of the 25 Ah NCM battery.

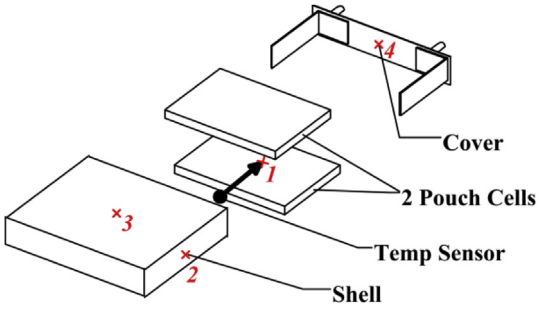

Fig. 4. The positions of the thermocouples.

pouch cells remain intact so that it is an in situ measurement of the internal temperature within the battery.

Some other thermocouples are fixed surrounding the whole battery. Their positions are marked in red in Fig. 4 and listed in Table 1.

After the thermocouple No. 1 is inserted in the battery, the battery is re-assembled and ready for the thermal runaway test in the EV-ARC, Fig. 5. The K type thermocouples are provided by Pico Technology and connected to a data logger, while the N type thermocouple is the sensor of the ARC. The sampling time interval of the data logger is set as one second.

Note that the voltage is also monitored during the test, Fig. 5. To study the behavior of the internal resistance, a pulse charge/discharge profile (Fig. 6) is exerted during the thermal runaway process for one of the series tests.

All of the experiments conducted using the EV-ARC are listed in Table 2. Experiment No. 1 is conducted for the primary analysis of the thermal runaway features of the large format lithium ion battery. Experiment No. 2 is for the evaluation of the internal resistance using a pulse charge/discharge profile in Fig. 6. Experiment No. 3 and No. 4 are done for comparison with different temperature rate sensitivities.

2.4. The test of the separator using differential scanning calorimetry

The separator of the 25 Ah battery is polyethylene (PE) based with ceramic coating manufactured by the AE Energy. A ramp heating test was conducted by differential scanning calorimetry (DSC) and thermogravimetric analysis (TGA), because the thermal behavior of the separator influences the thermal runaway performance of the 25 Ah NCM battery. The DSC/TGA measurements were carried out with a STA 409 PC/4/H Luxx® manufactured by Netzsch, Germany, as in Ref. [36]. The measured parameters used are presented in Table 3.

Table 1
Settings of the thermocouples shown in Fig. 4.

No.	Name	Position	Thermocouple type
1	TC_1	At the center between the two pouch cells	K type
2	TC_2	At the center of the narrow side surface on the shell	K type and N type for the ARC
3	TC_3	At the center of the broad side surface on the shell	K type
4	TC_4	At the vent valve	K type

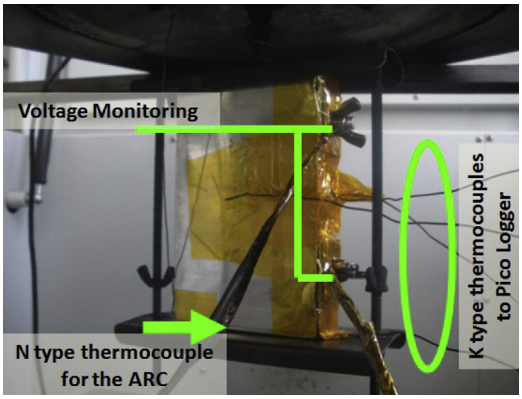

Fig. 5. The settings for the EV-ARC test.

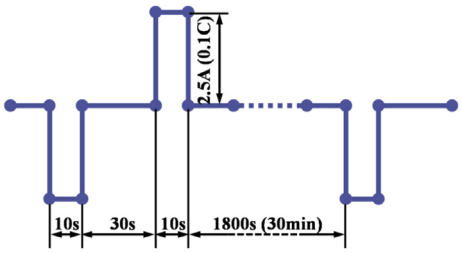

Fig. 6. The pulse charge/discharge profile.

3. Results and discussion

3.1. The DSC/TGA test result of the separator

The endothermic peak of the DSC test for the PE-based separator locates at around 130–140 °C [37–40], indicating the melting point of the PE-based separator. For the test done in this paper, the specific PE-based separator has an endothermic peak locating at 139.8 °C with an onset temperature of 127.3 °C and an enthalpy of −39.73 J g^{-1}, calculated by the instrument, Fig. 7. The PE-based

Table 2
All of the experiments conducted by the EV-ARC.

Exp. No.	Temperature rate sensitivity/°C min^{-1}	Internal thermocouple	Usage
1	0.01	√	Primary analysis
2	0.01	√	Internal resistance
3	0.02	√	For comparison
4	0.02	×	For comparison

Table 3
The measured parameters of the DSC.

Settings	Description
Heating rate	10 K min^{-1}
Temperature range	20–400 °C
Inert gas	Argon, flow rate: 60 mL min^{-1}
Sample crucible	Al_2O_3
Calibration test	Al_2O_3-standard, temperature, sensitivity

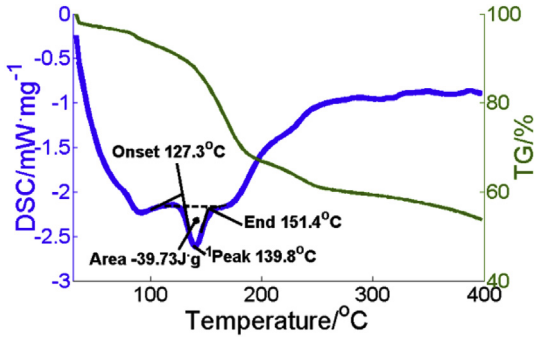

Fig. 7. The DSC/TGA result of the separator.

separator made by the AE Energy melts at around 140 °C. The separator with ceramic coating does not lose integrity until about 250 °C when the voltage drops sharply indicating a breakdown behavior and internal short circuit. Micro internal short circuit occurs between 140 °C and 250 °C [41].

3.2. Experiment No. 1, the primary test

3.2.1. The stages of the thermal runaway of the lithium ion battery

Experiment No. 1 is the primary test that is analyzed in detail. The real-time voltage and temperature value of different thermocouples are drawn in Fig. 8. The TC_1–TC_4 indicate the temperature values of the thermocouple No. 1–No. 4. The maximum temperature during the test is 853.5 °C reported by TC_1, which is the internal temperature of the battery. Fig. 9 illustrates the temperature rate vs. temperature curve, which is the differentiation of the TC_1 data smoothed by the moving average algorithm. Fig. 9 is also called the phase diagram of the temperature in the field of control theory.

The temperature rises exponentially when thermal runaway happens. The temperature curve displays an approximately vertical line in Fig. 8. The sharp rise of the temperature is shown in Fig. 10 magnified from Fig. 8. The rising period of the temperature can be divided into two stages. The temperature increases much more rapidly before 750 °C than it does after 750 °C.

Considering the results of Figs. 8–10 and the existing literature, the thermal runaway process can be divided into 6 Stages with 3 critical temperatures (T_1, T_2 and T_3), as shown in Figs. 8 and 9. Reactions that happen on different stages for the tested NCM battery are marked in Fig. 11.

Stage I: The capacity fades at high temperature. The Li-ion de-intercalates from anode [42–49].
Stage II: T_1 is the onset temperature of detectable self-heating and the start temperature of Stage II. T_1 is influenced by the temperature rate sensitivity set in EV-ARC: a higher accuracy of temperature rate sensitivity corresponds with a lower onset temperature. In Stage II, the capacity continues fading at higher temperature, the SEI decomposition happens [8,9,50–53]. Losing its protection layer the anode starts to react with the electrolyte and releases detectable heat [8,37,51].
Stage III: T_2 is the start temperature of Stage III, the progress of the temperature rise slows down due to the separator melting as discussed in Section 3.1.
Stage IV: Accelerating process starts with micro short circuit inside. The anode reaction continues consuming active material in the negative electrode. Though in general acknowledgment, the cathode material should have started to react at this stage, [28,50,54,55], the NCM cathode seems to be strong enough not to react until the temperature reaches 240 °C or higher [56–61].
Stage V: T_3 is the start temperature of Stage V, when the temperature starts to go up exponentially. Note that the temperature is recorded once per second like those listed in Table 4. The T_3 is defined as the temperature $T(k)$, when the difference of $T(k)$ and $T(k-1)$ is higher than 1 °C s^{-1}, Eqn. (1). $T(k)$ is the temperature recorded by the thermocouple with a frequency of one point per second. k is the time serial number of the test. For example, for the fragments of the TC_1 value in Table 4, the T_3 is 259.0 °C.

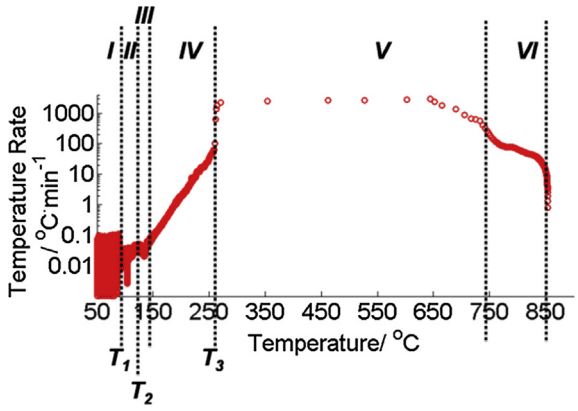

Fig. 9. Phase diagram of T of the Experiment No. 1.

$$T_3 = T(k), \text{when} T(k) - T(k-1) > 1\,^{\circ}\text{C}\,\text{s}^{-1},\ (k = 1,2,3\ldots) \quad (1)$$

In the Stage V, the separator loses its whole integrity, fierce short circuit occurs, reactions such as the NCM cathode decomposition [56–61], electrolyte decomposition [62–64] and PVDF decomposition [37,50,65] happens, and energy releases instantly. Note that the EV-ARC turns to the cooling mode to protect the container when the value of the EV-ARC sensor, TC_2, reaches 450 °C.

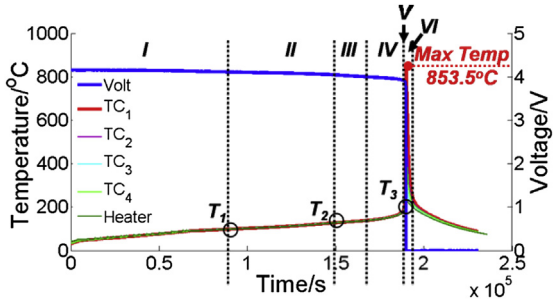

Fig. 8. (T,V)–t curve of the Experiment No. 1.

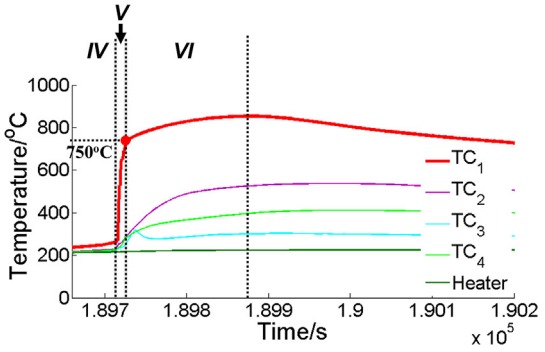

Fig. 10. The magnified figure of Fig. 8 to illustrate the boundary between Stage V and VI.

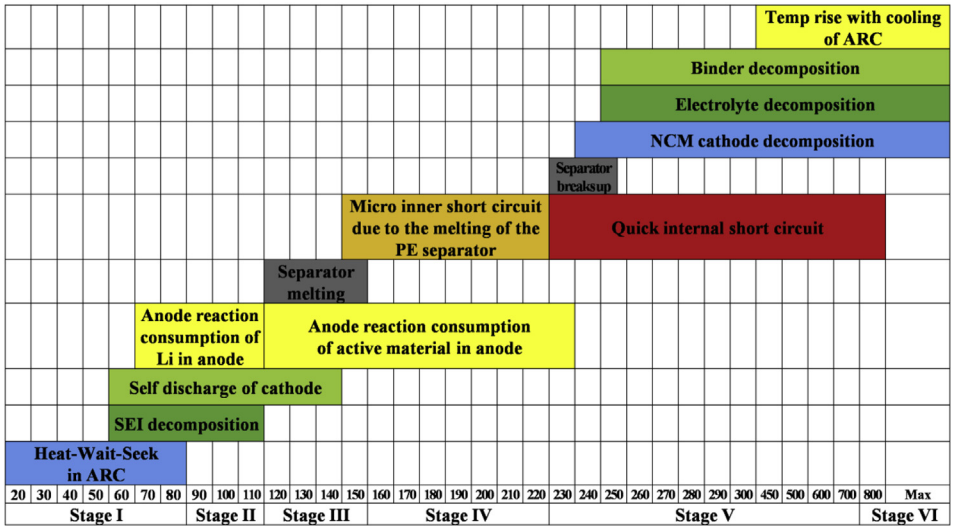

Fig. 11. Temperature ranges for different stages of thermal runaway test using EV-ARC.

Table 4
Fragments of the TC_1 value.

Time (k)	189,706	189,707	189,708	189,709	189,710	189,711	189,712	189,713	189,714	189,715	189,716
TC_1/°C	256.2	257.1	258.0	**259.0**	260.0	261.4	263.0	264.1	271.0	353.5	462.5

The number 259.0 in bold is used to demonstrate the definition of T_3. T_3 is the start temperature of the Stage V during thermal runaway. T_3 is defined in Eqn. (1).

Stage VI: The residual reactions continue bringing the temperature a little higher, from about 750 °C to the maximum, with the cooling process of the EV-ARC. In Stage VI, the temperature rate is much lower than that in Stage V

3.2.2. The temperature difference within the large format battery

As discussed in the introduction, the temperature difference within the battery is less than about 10 °C as reported in Refs. [31–34], while for thermal runaway triggered by an internal short circuit it is as high as approximate 600 °C [28]. The recorded temperatures of the 4 thermocouples listed in Table 1 are used to analyze the temperature distribution within the battery during the test. As a magnified picture of Figs. 8 and 12(a) shows the temperature curves of TC_1–TC_4. The temperature difference among the 4 thermocouples is quite small during the self-heating process.

Define a variable named MTD, representing the maximum temperature difference as in Eqn. (2). l is the time serial number of the test data, while i and j is the number of the thermocouple as in Table 1.

$$\mathrm{MTD}(l) = \mathrm{Max}\{|TC_i(l) - TC_j(l)|\}, \quad (i,j = 1,2,3,4;\ l = 1,2,3\ldots) \tag{2}$$

Fig. 12(b) shows the MTD–T curve during the test. The temperature used for curving is the value of TC_1. The MTD is not as high as 1 °C until the temperature reaches 161.5 °C, which takes about 184,000 s. As the thermal runway occurs at about 190,000 s, it means that the MTD maintains lower than 1 °C for 184,000/190,000 = 97% of the whole test. What's more, from that point the temperature of TC_1 starts to take the lead and rise much faster than the others do.

3.2.3. The interval between the voltage drop and the temperature rise

During the experiment, it is observed that the sharp drop of the voltage occurred a little sooner than the instantaneous rise of the temperature, Fig. 13. $\Delta t_{V,T}$ is defined to describe the interval between the voltage drop and the temperature rise, as in Eqn. (3). The

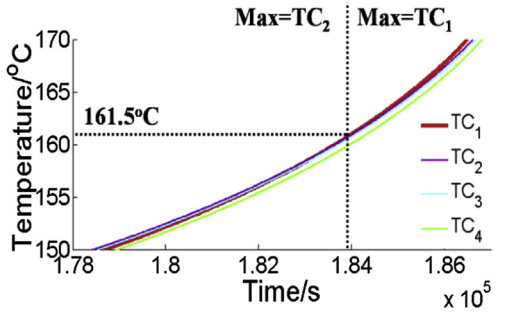

(a) The magnified figure of Fig. 8 to illustrate the temperature distribution within the battery.

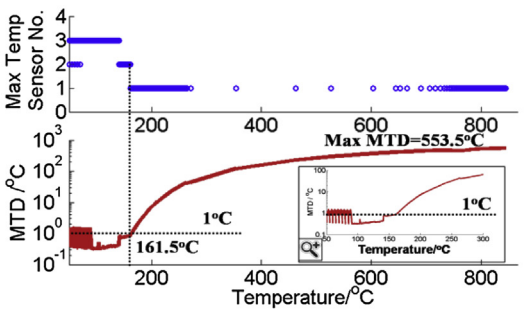

(b) The maximum temperature difference of the 4 thermocouples.

Fig. 12. The temperature difference within the large format battery. (a) The magnified figure of Fig. 8 to illustrate the temperature distribution within the battery. (b) The maximum temperature difference of the 4 thermocouples.

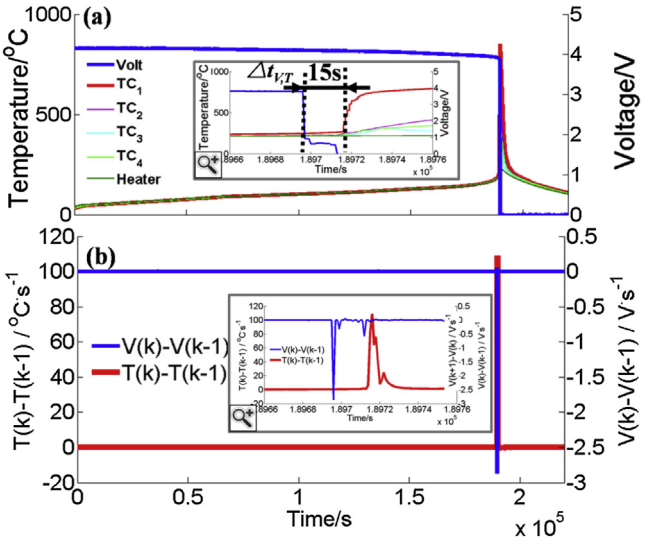

Fig. 13. The interval between the voltage drop and the temperature rise.

variable m and n are the time serial numbers of the test data. For the result in Fig. 13(b), $m = 189{,}878$ and $n = 189{,}893$. Therefore, for the result of Experiment No. 1, $\Delta t_{V,T} = 189{,}893 - 189{,}878 = 15$ s. The interval between the voltage drop and the temperature rise provides a possible way to predict the occurrence of the coming thermal runaway.

$$\Delta t_{V,T} = n - m,$$
where $m : V(m-1) - V(m) > 3\ \mathrm{V\ s^{-1}}; n : T(n) - T(n-1) > 1\ ^{\circ}\mathrm{C\ s^{-1}} (m, n = 1, 2, 3\ldots)$

3.3. The variation of the internal resistance during the thermal runaway test

As discussed in Section 3.1, the shutdown process carries a possible increase of internal impedance [38–40]. The variation regulation of the internal resistance during the thermal runaway test has been studied using a test profile proposed in Fig. 6. The voltage curve employs many discharge/charge periods, Fig. 14(a). The internal resistance R_{in} is defined as the quotient of the average pulse voltage and the pulse current, as in Eqn. (4). The voltage pulse of discharge is ΔV_1, the voltage pulse of charge is ΔV_2 and the pulse current is $\Delta I = 2.5$ A, set in Fig. 6. The initial R_{in} is 20 mΩ, as in Fig. 14(b). Then the R_{in} rises slowly to 60 mΩ before the thermal runaway happens. At around 250 °C, the separator loses its integrity, so that the thermal runaway happens due to massive internal short circuit. Correspondingly, the battery swells and R_{in} rises to 370 mΩ.

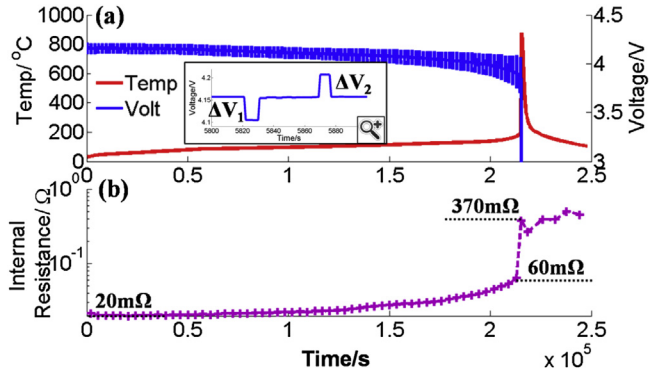

Fig. 14. The variation of the internal resistance during the thermal runaway test.

$$R_{in} = (\Delta V_1 + \Delta V_2)/2\Delta I \tag{4}$$

3.4. The comparison tests

Comparison tests are done as in Table 2. Fig. 15 compares the values of TC_2 of the different tests. Note that for the Experiment No. 1–No. 3, relative results in Table 2 are acquired from TC_1 based on the definition proposed in the former sections. However, because the Experiment No. 4 is done without thermocouple inserted inside the battery, relative results in Table 2 for the Experiment No. 4 are derived from TC_2.

The range of the onset temperature T_1 is from 85 °C to 105 °C, which matches the reaction range of the SEI decomposition in Refs. [1–6]. The critical temperatures for different experiments, i.e. T_1, T_2 and T_3 are collected in Table 5. Their values look similar to each other with some minor variations. T_{max} is the maximum temperature of the TC_1 in Table 5, column 6. The T_{max} for the different experiments seem to be as high as 870 °C or so. The MTD_{max} is the maximum MTD during the tests as in Table 5. The MTD_{max} reflects the maximum temperature difference between the internal temperature and the surface temperature when thermal runaway happens. All of the MTD_{max}s seem to be as high as 520 °C or so. Note that the simulated temperature difference for thermal runaway triggered by an internal short circuit is approximately 600 °C in Ref. [28].

The time-consumptions of the 4 experiments vary from each other. A variable Δt_{TR} is defined to describe the time interval that each experiment takes from Stage III to Stage VI, as in Eqn. (5), Fig. 15. r is the time serial number when the temperature reaches its highest, while s is the time serial number when the temperature reaches the melting point of the separator, i.e. 120 °C. The Δt_{TR}s are also collected in Table 5. It takes about 54,000 s for Experiment No. 1 and No. 2 to go from Stage III to Stage VI, while it takes about 77,000 s for Experiment No. 3 and No. 4.

$$\Delta t_{TR} = r - s:$$
$$\text{where}, r : TC_1(r) = T_{max}; s : TC_1(s) = 120\,^{\circ}\mathrm{C}.\ (r, s = 1, 2, 3\ldots). \tag{5}$$

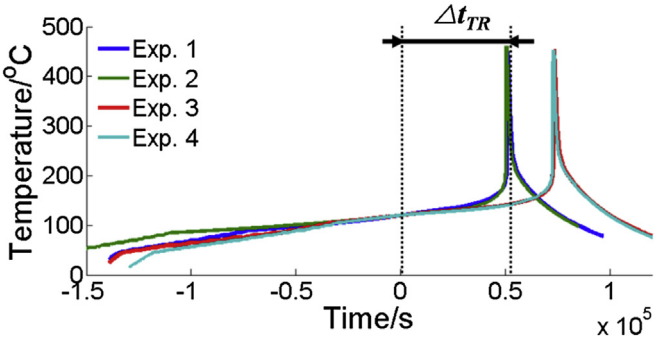

Fig. 15. Comparison of Δt_{TR} of different EV-ARC heating tests.

Table 5
Critical statistics of different experiments for comparison.

Exp. No.	T_1/°C	T_2/°C	T_3/°C	$\Delta t_{V,T}$/s	T_{max}/°C	MTD_{max}/°C	Δt_{TR}/s
1	90	124	259	15	854	553	54,210
2	85	122	254	30	876	524	53,820
3	105	122	240	27	877	523	77,220
4	105	120	224	41	–	–	76,800

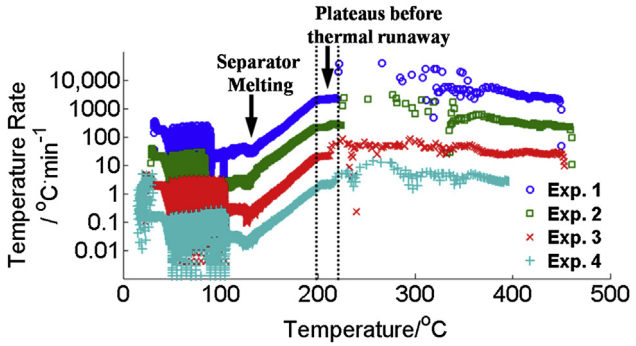

Fig. 16. The comparison of temperature rates.

Fig. 16 illustrates the temperature rate vs. temperature curve, which is the differentiation of the TC_2 data smoothed by the moving average algorithm. Adjacent curves are shifted by multiplying a factor of 10. The valleys of the curve at around 130 °C indicate the melting of the separator. Plateaus can be observed before thermal runaway suggesting the internal short circuit between the voltage shutdown and the temperature rise, or the $\Delta t_{V,T}$.

3.5. The residuals

The samples have been disassembled after tests. The residuals for all of the 4 samples look the same. The sample has swelled and looks like a mess after opening the cover of the EV-ARC, Fig. 17(a). The ashes of the two pouch cells have been extracted, Fig. 17(b). The aluminum foil remains covering the core, indicating the outside temperature has not reached the melting point of the aluminum foil, 660 °C, during the test. The book like core has been opened, Fig. 17(c) and (d). No intact aluminum electrode foil but some gray fragments have been found inside the samples indicating that the internal temperature is higher than the melting point of the aluminum foil.

4. Conclusion

In this paper, a type of 25 Ah prismatic battery with $Li(Ni_xCo_yMn_z)O_2$ (NCM) cathode is tested by the EV-ARC. The thermal runaway features of the 25 Ah battery have been analyzed synthetically.

The internal temperature has been recorded and the temperature difference within the battery during the thermal runaway process has been reported. The temperature inside the battery when thermal runaway happens is as high as 870 °C or so, much higher than that outside the battery. So it is meaningful to study the internal temperature for the large format battery. The temperature difference within the battery stays lower than 1 °C for most of the test time. The temperature difference increases as the test goes on, and it rises to its highest (about 520 °C) when thermal runaway happens. The measured temperature data is beneficial for building thermal abuse models of a large format lithium ion battery.

The battery voltage is recorded and the internal resistance is measured by exerting a pulse current profile on the sample during

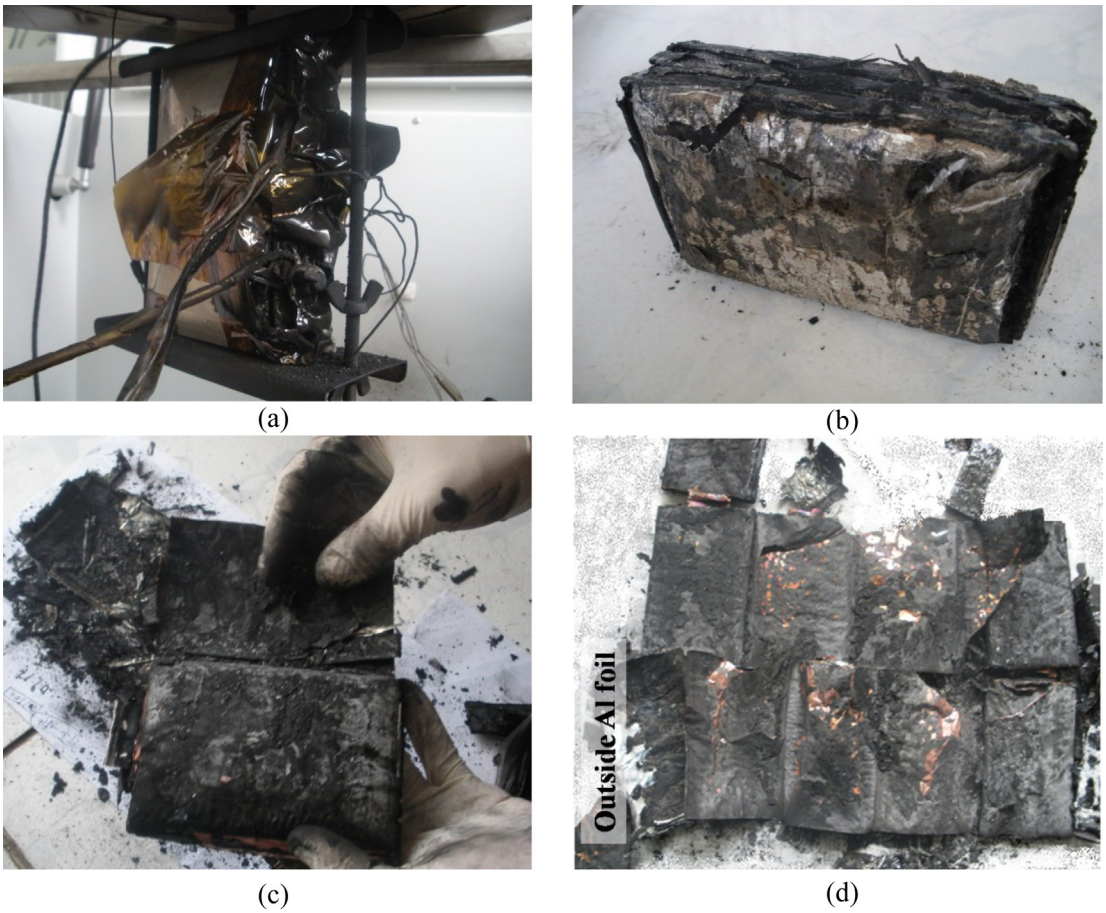

Fig. 17. The residuals of the samples.

the EV-ARC test. The time interval between the sharp shutdown of the voltage and the exponential rise of the temperature is observed. It takes about 15–40 s from the voltage drop to the temperature rise. Such a time interval is good for a possible early warning of the battery thermal runaway. In addition, the internal resistance increases slowly from 20 mΩ to 60 mΩ before thermal runaway. When thermal runaway happens, the internal resistance rises to 370 mΩ indicating the loss of integrity of the separator or the swell of the pouch cells.

Further work will focus on the thermal runaway model of the large format prismatic lithium ion battery and on the enthalpy released during the runaway process to evaluate the probability of the thermal runaway propagation to adjacent batteries.

Acknowledgments

This work is funded by the MOST (Ministry of Science and Technology) of China under the contract of No. 2010DFA72760 and No. 2011CB935902, and also funded by the NSFC (National Natural Science Foundation) of China under the contract of No. 61004075. It is also funded by the Tsinghua University Initiative Scientific Research Program (Grant No. 2011THZ01004).

The author would like to thank Mr. Maogang Li from Thermal Hazard Technology for the technological support. And the author would also thank Mr. Hengwei Liu for the maintenance of the EV-ARC.

References

[1] Q.S. Wang, P. Ping, X. Zhao, et al., J. Power Sources 208 (2012) 210–224.
[2] R. Spotnitz, J. Franklin, J. Power Sources 113 (2003) 81–100.
[3] T.M. Bandhauer, S. Garimella, T.F. Fuller, J. Electrochem. Soc. 158 (3) (2011) 1–25.
[4] D. Lisbona, T. Snee, Process Saf. Environ. Prot. 89 (2011) 434–442.
[5] J. Wen, Y. Yu, C. Chen, Mater. Express 2 (3) (2012) 197–212.
[6] L. Lu, X. Han, J. Li, J. Hua, M. Ouyang, J. Power Sources 226 (2013) 272–288.
[7] The Accelerating Rate Calorimeter (EV-ARC) Operations Manual Version 1, Thermal Hazard Technology, April 2010.
[8] M.N. Richard, J.R. Dahn, J. Electrochem. Soc. 146 (6) (1999) 2068–2077.
[9] D.D. Macneil, D. Larcher, J.R. Dahn, J. Electrochem. Soc. 146 (10) (1999) 3596–3602.
[10] J. Jiang, J.R. Dahn, Electrochem. Commun. 6 (2004) 31–43.
[11] Y.D. Wang, J.W. Jiang, J.R. Dahn, Electrochem. Commun. 9 (2007) 2534–2540.
[12] E.P. Roth, SAE Int. J. Pass. Cars – Mech. Syst. 1 (1) (2008) 326–332.
[13] J.R. Selman, S.A. Hallaj, I. Uchida, Y. Hirano, J. Power Sources 97–98 (2001) 726–732.
[14] E.P. Roth, D.H. Doughty, J. Power Sources 128 (2004) 308–318.
[15] H. Ishikawa, O. Mendoza, Y. Sone, M. Umeda, J. Power Sources 198 (2012) 236–242.
[16] C.Y. Jhu, Y.W. Wang, C.M. Shu, et al., J. Hazard. Mater. 192 (2011) 99–107.
[17] C.Y. Jhu, Y.W. Wang, C.Y. Wen, et al., Appl. Energy 100 (2012) 127–131.
[18] C.Y. Wen, C.Y. Jhu, Y.W. Wang, et al., J. Therm. Anal. Calorim. 109 (2012) 1297–1302.
[19] T.Y. Lu, C.C. Chiang, S.H. Wu, et al., J. Therm. Anal. Calorim. 114 (3) (April 2013) 1083–1088.
[20] C.Y. Jhu, Y.W. Wang, C.Y. Wen, et al., J. Therm. Anal. Calorim. 106 (2011) 159–163.
[21] M.S. Wu, C.Y. Liu, Y.Y. Wang, et al., Electrochim. Acta 52 (2006) 1349–1357.
[22] A. Smyshlyaev, M. Krstic, N. Chaturvedi, et al., in: American Control Conference on O'Farrell Street, San Francisco, CA, USA, 2011, June 29–July 01, pp. 959–964.
[23] G.J. Offer, V. Yufit, D.A. Howey, et al., J. Power Sources 206 (2012) 383–392.
[24] Y. Zheng, L. Lu, X. Han, et al., J. Power Sources 226 (2013) 33–41.
[25] M. Dubarry, B.Y. Liaw, M.S. Chen, et al., J. Power Sources 196 (2011) 3420–3425.
[26] H. Haruna, S. Itoh, T. Horiba, et al., J. Power Sources 196 (2011) 7002–7005.
[27] K.J. Lee, K. Smith, A. Pesaran, et al., J. Power Sources 241 (2013) 20–32.
[28] G.H. Kim, A. Pesaran, R. Spotnitz, J. Power Sources 170 (2007) 476–489.
[29] G.H. Kim, K. Smith, J. Ireland, A. Pesaran, J. Power Sources 210 (2012) 243–253.
[30] X. Lin, H.Z. Perez, J.B. Siegel, et al., IEEE Trans. Control Syst. Technol. 21 (5) (2013) 1745–1755.
[31] C.Y. Lee, S.J. Lee, M.S. Tang, et al., Sensors 11 (2011) 9942–9950.
[32] G. Zhang, L. Cao, S. Ge, et al., In situ measurement of Li-ion battery internal temperature, Abstract #538, 224th ECS Meeting, The Electrochemical Society.
[33] C. Forgez, D.V. Do, G. Friedrich, et al., J. Power Sources 195 (2010) 2961–2968.
[34] Z. Li, J. Zhang, B. Wu, et al., J. Power Sources 241 (2013) 536–553.
[35] D.H. Doughty, Vehicle Battery Safety Roadmap Guidance, Oct. 2012, pp. 65–66.
[36] X.M. He, L. Wang, W.H. Pu, et al., J. Therm. Anal. Calorim. 94 (1) (2008) 151–155.
[37] P. Biensan, B. Simon, J.P. Peres, et al., J. Power Sources 81–82 (1999) 906–912.
[38] P. Arora, Z. Zhang, Chem. Rev. 104 (2004) 4419–4462.
[39] B.N. Pinnangudi, S.B. Dalal, N.K. Medora, et al., in: IEEE Symposium on Product Compliance Engineering (ISPCE), 2010.
[40] C.J. Orendorff, The Role of Separators in Lithium-ion Cell Safety, The Electrochemical Society Interface, Summer, 2012, pp. 61–65.
[41] Private communication, J.G. Cheng from AE Energy, June, 7, 2013.
[42] K. Takei, K. Kumai, Y. Kobayashi, et al., J. Power Sources 97–98 (2001) 697–701.
[43] R.D. Ramasamy, R.E. White, B.N. Popov, J. Power Sources 141 (2005) 298–306.
[44] Q. Zhang, R.E. White, J. Power Sources 173 (2007) 990–997.
[45] K. Amine, J. Liu, S. Kang, et al., J. Power Sources 129 (2004) 14–19.
[46] K. Amine, J. Liu, I. Belharouak, Electrochem. Commun. 7 (2005) 669–673.
[47] Q. Zhang, R.E. White, J. Power Sources 179 (2008) 785–792.
[48] R. Yazami, Y. Ozawa, J. Power Sources 153 (2006) 251–257.
[49] R. Yazami, Y.F. Reynier, Electrochim. Acta 47 (2002) 1217–1223.
[50] H. Maleki, G. Deng, A. Anani, J. Howard, J. Electrochem. Soc. 146 (9) (1999) 3224–3229.
[51] Z. Zhang, D. Fouchard, J.R. Rea, J. Power Sources 70 (1998) 16–20.
[52] M.H. Ryou, J.N. Lee, D.J. Lee, et al., Electrochim. Acta 83 (2012) 259–263.
[53] Q.S. Wang, J. Sun, X. Yan, C. Chen, Thermochim. Acta 487 (2005) 12–16.
[54] D.D. Macneil, J.R. Dahn, J. Phys. Chem. A. 105 (2001) 4430–4439.
[55] H. Arai, M. Tsuda, K. Saito, et al., J. Electrochem. Soc. 149 (4) (2002) 401–406.
[56] H.Y. Wang, A.D. Tang, K.L. Huang, Chin. J. Chem. 29 (2011) 1583–1588.
[57] H. Kim, M. Kong, K. Kim, et al., J. Power Sources 171 (2007) 917–921.
[58] H. Kim, K. Kim, S.I. Moon, et al., J. Solid State Electrochem. 12 (2008) 867–872.
[59] I. Belharouak, Y.K. Sun, J. Lin, K. Amine, J. Power Sources 123 (2003) 247–252.
[60] J. Jiang, K.W. Eberman, L.J. Krause, J.R. Dahn, J. Electrochem. Soc. 152 (3) (2005) 566–569.
[61] Y.H. Chen (Ph. D Thesis), Investigation on $LiCo_{1/3}Ni_{1/3}Mn_{1/3}O_2$ Cathode Material and Safety of Lithium-ion Battery, College of Chemical Engineering, Tianjin University, China, Tianjin, Dec. 2006, p. 50 (in Chinese).
[62] S.E. Sloop, J.K. Pugh, S. Wang, et al., Electrochem. Solid-state Lett. 4 (4) (2001) 42–44.
[63] G.G. Botte, R.E. White, Z.M. Zhang, J. Power Sources 97–98 (2011) 570–575.
[64] T. Kawamura, A. Kimura, M. Egashira, et al., J. Power Sources 104 (2002) 260–264.
[65] A.D. Pasquier, F. Disma, J.M. Tarascon, et al., J. Electrochem. Soc. 145 (2) (1998) 472–477.